6

Low-Frequency Linacs and Compressors

Contents

6.1 Introduction

The NLC complex has seven S-band linacs and four L-band linacs. The main L-band linac accelerates the positron beam from the positron target to 2 GeV where it enters the damping ring. In addition there are one 80-MeV L-band linac associated with the positron energy compressor at the output of the positron booster linac and two 134-MeV L-band linacs associated with the electron and positron first stage compressors at the output of the two damping rings. These linacs are run in phase quadrature with the beam to introduce the linear correlation between time and energy within each bunch which is required for compression. The seven S-band linacs are:

1) The Positron Drive Linac which accelerates the electrons which strike the positron target.
2) The Electron Booster Linac which accelerates the electron beam to 2 GeV where it enters the Electron Damping Ring.
3) 42-MeV electron energy compressor at the output of the electron booster linac.

4,5) The Electron and Positron Preaccelerators which accelerate the beams from the damping rings to 10 GeV where the second bunch compression occurs.

6,7) 3.85-GeV S-band linacs to produce the linear energy correlation required for each of the second-stage compressors.

These linacs share enough common characteristics and design problems that it is appropriate to discuss the rf design of these linacs together in this chapter. The principal design issues confronting the rf design of these linacs are beam loading and dipole wakefields. Except for the first 250-MeV portion of the Positron L-band linac which is inside a 0.5-T solenoid, all of these linacs must be capable of accelerating about 2-A beams with about 100-ns macropulse length. The part of the Positron L-band linac inside the solenoid needs to accelerate a total effective current of about 14 A since both electrons and positrons get captured onto their respective accelerating crests, $\lambda/2$ apart. Because the electrons are produced by ionization as well as by pair production, there are about 65% more electrons than positrons. Furthermore, the solenoid transports many particles which are outside the phase and energy range acceptable to the pre-damping ring. These excess particles will be scraped off in the energy analyzing slits after the bend immediately after the solenoid, but in the two capture sections within the solenoid they create extremely heavy beam loading.

6.2 Beam-Loading Compensation

All of these linacs are fairly heavily loaded by a beam with a pulse length much shorter than the reasonable filling times of the structures, which are in turn shorter than the ringing time, $2Q/\omega$, for the structure. In this situation, the energy of the beam will drop approximately linearly with time during the pulse as a result of beam loading. For this case there are two natural choices for beam-loading compensation: 1) ΔT (or Early Injection), *i.e.*, injecting the beam into the structure before the structure is full; 2) ΔF, *i.e.*, having one or more accelerator structures running at a frequency 1 to 2 MHz above or below the nominal frequency and roughly in phase quadrature from the accelerating phase. Thus the beginning of the pulse can be decelerated by the off-frequency section(s), while the end of the pulse is accelerated. The advantage of ΔT compensation is that the compensation occurs in every accelerator section, so that the energy spectrum can be good throughout the linac, thus minimizing emittance growth from dispersion and chromatic effects.

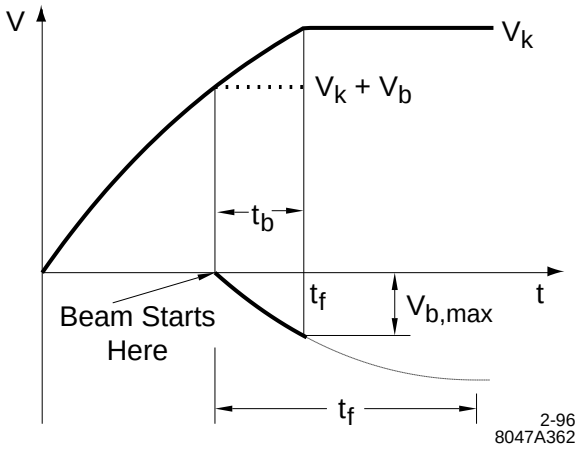

Figure 6-1. *ΔT beam-loading compensation for rectangular rf input pulse.*

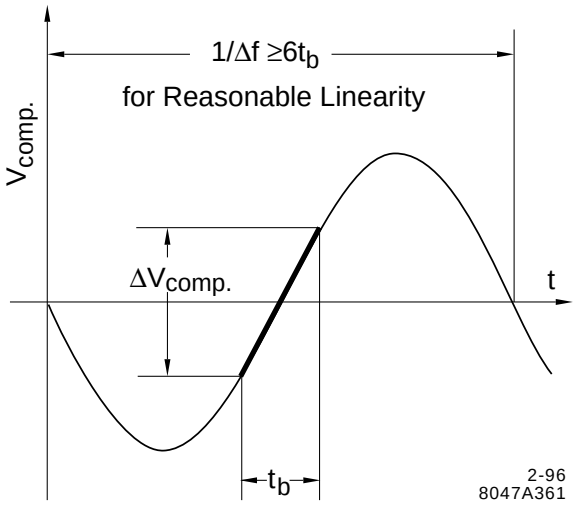

Figure 6-2. *Energy gain, $V_k(t)$, in a ΔF compensation section.*

The way ΔT compensation works is shown in Figure 6-1 in which the voltage $V_k(t)$ produced by a step-function rf pulse is plotted as a function of time for a traveling-wave linac section. Also plotted is the beam-induced voltage $V_b(t)$. The resultant sum of $V_k(t)$ and $V_b(t)$ is plotted for the case where the beam is turned on before the linac structure is full. To illustrate the principle of ΔF compensation, the voltage gain $V_{\rm comp}(t)$ of a beam with an F_0 bunch structure in a ΔF-compensation section operating at a frequency $F_0 \pm \Delta$F is plotted in Figure 6-2. The beam is bunched with a bunch-repetition frequency of 714 MHz, a subharmonic of the accelerator frequency F_0. In an accelerator section powered by rf at a frequency $F_0 \pm \Delta F$, the bunches see a field which appears to vary with the difference frequency ΔF as shown in Figure 6-2. If the beam pulse length satisfies the relation $t_b \leq \frac{1}{6\Delta F}$ and is phased as shown, the energy gain will vary quite linearly with time.

It is instructive to calculate the power required for compensation by early injection for a rectangular rf pulse (non-sledded) in the approximation that $t_b << t_f << 2Q/\omega$, where t_b is the beam pulse length and t_f is the structure

filling time.

$$\frac{dV_b}{dt} = -\frac{i}{2}\frac{\omega r}{Q}L \tag{6.1}$$

$$\frac{dV_k}{dt} = \left(\frac{P v_g \omega r}{Q}\right)^{1/2} \tag{6.2}$$

$$V_k^2 = L^2 \frac{P}{v_g}\frac{\omega r}{Q} \tag{6.3}$$

where V_b= beam-induced voltage
i = beam current
L = accelerator length
V_k= voltage produced by klystron power
P = klystron power
v_g= average group velocity in the structure

Setting $\frac{dV_k}{dt} = -\frac{dV_b}{dt}$ and multiplying by Eq. 6.3 we find that

$$P = \frac{iV_k}{2} \tag{6.4}$$

This remarkable result says that for compensation by early injection the klystron power has to be approximately equal to half the power absorbed by the beam *and is independent of the shunt impedance of the structure and the length of the linac* under the inequalities stated above. For compensation by early injection with the approximation used here the filling time must satisfy the relation:

$$\frac{t_b}{t_f} = \frac{V_b}{V_k} \tag{6.5}$$

With ΔF compensation one is free to pick the filling time. In the approximation that $t_b << t_f$, and that r/Q is independent of group velocity, the beam-induced voltage is independent of filling time (see Eq. 6.1). For filling times short compared with $2Q/\omega$ the peak power required varies inversely with filling time. One can also reduce the power required by decreasing the gradient. For a given required voltage, the power varies linearly with gradient, however the beam-induced voltage varies linearly with length or inversely with gradient. Increasing the beam-induced voltage tightens the tolerance on the compensation and increases the fraction of the overall length and the fraction of the total rf power which must be dedicated to the off-frequency compensating sections. One finds that for either ΔT or ΔF compensation there is an optimum product Lr/Q which minimizes the power required for accelerating the beam to a given voltage and compensating for beam loading. The optimum is very broad and changing the product by a factor of two in either direction only raises the power required by about 15%. We have chosen an unloaded gradient of 25 to 30 MeV/m for the S-band accelerators to minimize dark current problems. This determines the length of the accelerator required for a given beam energy. For a fixed length the beam loading for a short pulse varies linearly with r/Q, so we pick a value about half of the optimum which increases the power required about the 15% mentioned above the minimum. With these choices the power and lengths required for ΔT compensation are somewhat greater (about 10%) than for ΔF. Our present feeling is that the ΔF system is probably easier to operate. Depending on the percentage beam loading and the energy spread after compensation, a total phase shift of 1/2 to one radian is likely to be acceptable. Thus an off-frequency compensating section can correct for a beam-loading voltage V_b between 1/2 and one times the peak voltage of the section.

The principal disadvantage of the ΔF compensation, is that the beam energy spread reaches half of the compensation of a single off-frequency section. The compensation section then overcorrects by a factor of two which reverses

Frequency	2856 MHz
Structure type	DDS disk-loaded[a]
Structure length	3 m
# sections per module	4
Filling time	371 ns
Group velocity	0.05 c to 0.0125 c
# klystrons per module	2
Klystron power	65 MW
Rf pulse length (flattop)	4 μs
Pulse compression	SLED I

[a] Damped Detuned Structure

Table 6-1. *S-band linac rf parameters.*

correlation of energy with time during the pulse. In order to maintain a small enough energy spread to achieve an acceptable emittance growth it appears necessary to distribute the power from one klystron running off frequency to a number of short accelerator sections, so that each correction is acceptably small. The compensation sections should be placed so that the beam-loaded particles have the same total betatron phase advance as the first particles in the bunch train which have no beam loading. This is approximately equivalent to saying that they should spend as much time (or distance along the accelerator axis) high in energy as they do low in energy. That is the spatial average along the accelerator axis of the difference in energy between the first particle and the last particle should vanish. One can either choose to have short ΔF sections after each regular sections or to have one or two long ΔF sections in each of the accelerator modules. It appears to us that the high power microwave distribution system to many short ΔF compensation sections becomes unreasonably complicated and expensive. Using long ΔF sections will, however, result in poor energy spectrum and associated emittance growth. Therefore, we have chosen to use ΔT compensation for most of the low frequency linacs. The positron capture linac (inside the solenoid) requires ΔF compensation to achieve a acceptable multibunch energy spread because of the extremely high current. It is desirable to use ΔF compensation on the S-band bunch compressors, because the tuning to minimize the energy spread is very straightforward for ΔF compensation.

Table 6-1 presents the preliminary parameters for the S-band structure and rf system. The klystrons are assumed to be like the 65-MW 5045 klystrons, 240 of which power the existing SLAC linac. The useful power at the load is assumed to be 60 MW to allow for attenuation.

L-band Positron Linac: The initial acceleration of the positrons, from the target to the Positron Damping ring at 2 GeV, is done in a L-band linac with 1428-MHz rf power. The reason for this is that the four-dimensional phase space acceptance of a linac varies as λ^4. Thus, accelerating in a 1428-MHz linac instead of a 2856-MHz linac increases the phase volume acceptance of the linac by a factor of 16. This makes the production of the high-intensity ($\approx 10^{12}\ e^+$ per rf pulse) positron beam required for NLC comfortable for a conventional electromagnetic shower positron source. The beam-induced voltage per unit length for a beam pulse length much less than the filling time varies inversely as λ^2, so beam loading becomes less of a problem. 75-MW klystrons are used for accelerating the beam. For the first 200 MeV, the beam is focused by a solenoid. In this region we assume the beam loading is produced by a beam current of up to 14 A, since both electrons and positrons will be captured on the appropriate E field crests. The L-band linac rf parameters are given in Table 6-2.

Frequency	1428 MHz
Structure type	Gaussian detuned
Structure length	5 m
# sections per module	4
Filling time	675 ns
Group velocity	0.046 c to 0.0115 c
# klystrons per module	2
Klystron power	75 MW
Rf pulse length (flattop)	5 μs
Pulse compression	SLED I

Table 6-2. *L-band linac rf parameters.*

6.3 Numerical simulation of beam-loading compensation

The low-frequency linacs can be grouped into four groups based on their commonalities in structure and beam loading. In the following subsections we discuss the beam-loading compensation of each of the linac groups.

Two kinds of klystrons, S65 and L75, will be used to power the low-frequency linacs. The S65 klystron will be SLAC 5045 65-MW-like klystrons (see Section 6.4.1 for details), and capable of delivering 60-MW useful power, allowing for about 10% loss in the rf components. The L75 klystrons are L-band 75-MW klystrons (see Section 6.4.2 for details) which can deliver 67.5-MW useful power. We assume that the klystrons run at full power except when otherwise specified.

The numerical simulations in this section assume that the accelerator structures are dispersionless, which, we believe, is a good approximation. In this section, "energy spread" refers to the relative rms energy spread, and it is relative to the energy gain of that linac, except when other wise specified. The actual energy spread will be a factor of $\Delta E_{\rm gain}/(\Delta E_{\rm gain} + E_0)$ smaller, where E_0 is the initial beam energy. The energy spread obtained in this section is the residual of the beam-loading compensation. The total energy spread of the beam should be obtained by adding in quadrature the initial energy spread to the energy spread obtained in this section.

6.3.1 The e^+ Drive, the e^- Booster and the (e^-, e^+) Prelinacs

The e^+ drive linac, the e^- booster linac, and the (e^-, e^+) prelinacs use the same kinds of klystrons and acceleration structures. It is adequate to discuss the beam-loading compensation together in this section. The only differences among these linacs are the final energy and the beam current, as shown in Table 6-3. The acceleration structure will be S-band Damped Detuned Structure (DDS) ($F = 2.856\,$GHz). The beam-loading voltage is compensated by use of the ΔT compensation method.

The ΔT compensation requires that the beam be injected before the structure is full. The condition

$$\frac{dV_k}{dt} = -\frac{dV_b}{dt} \tag{6.6}$$

is essential for compensating the beam-loading voltage for the later bunches. The profile of the acceleration voltage, as a function of time, of a SLED-I driven structure is as shown in Figure 6-3. The bunch train occupies the region marked by the dotted lines. The slope of the voltage is inversely proportional to the filling time of the structure and

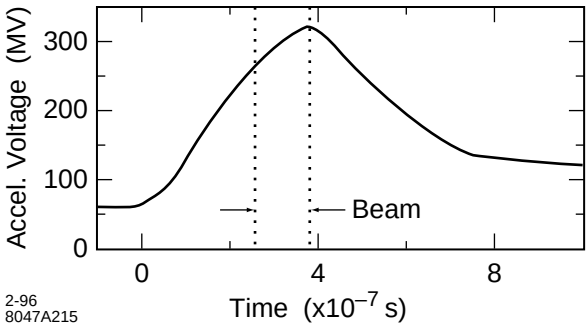

Figure 6-3. *Acceleration voltage of a SLED-I driven structure.*

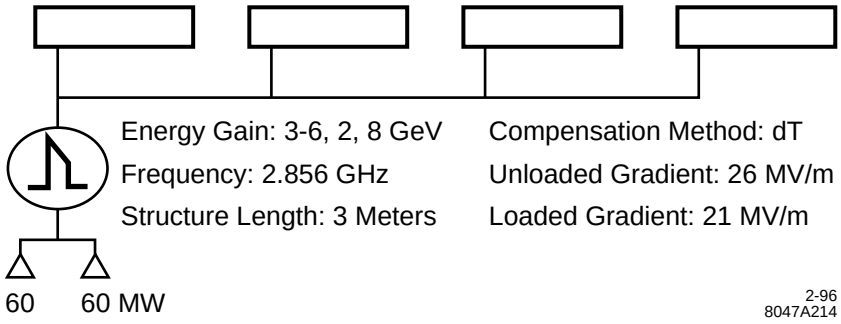

Figure 6-4. *An accelerator module for the e^+ drive, e^- booster, and the (e^-, e^+) prelinacs.*

depends on the profile of the SLED-I output. In order that Eq. 6.6 be satisfied, the filling time of the structure needs to be chosen properly, and the SLED output may also need to be modulated. The filling time of the structure in concern is chosen to be 0.371 μs, which is about three times the length of the bunch train. The beam loading is about 30% of the acceleration for a beam current of 2.2 A. Amplitude modulation of the SLED-I output is required to increase the derivative of the acceleration voltage. The amplitude modulation of the SLED-I output is obtained by amplitude modulating the klystron output. Our design uses a pair of klystrons to drive one SLED-I cavity. The phases of the two klystrons are modulated in opposite directions to obtain a combined amplitude modulated output. The klystrons will be S65 klystrons. A schematic drawing of an accelerator module is shown in Figure 6-4.

The energy spread due to the beam loading of a 2.2-A beam current can, in principle, be compensated to less than 2.4×10^{-5}, and less than 1.1×10^{-5} for a 1.5-A beam current. Since the energy spread is relative to the energy gain of the linac, the actual energy spread will be lower if the initial energy of the beam is not zero. The average gradients in the structure for the two cases are 17.3 MV/m and 21.2 MV/m respectively. The energy spectrum and the SLED-I wave form used for compensating the beam loading of a 2.2-A beam current are shown in Figure 6-5.

6.3.2 The e^+ Capture Linac

The accelerator structure for the e^+ capture linac will be detuned L-band structure (F=1.428 GHz) in order to have a large acceptance. The total energy gain of this linac is about 240 MeV. The beam is focused by a solenoid. We assume the beam loading in this linac is produced by a beam current of up to 14 A. For a typical disk-loaded L-

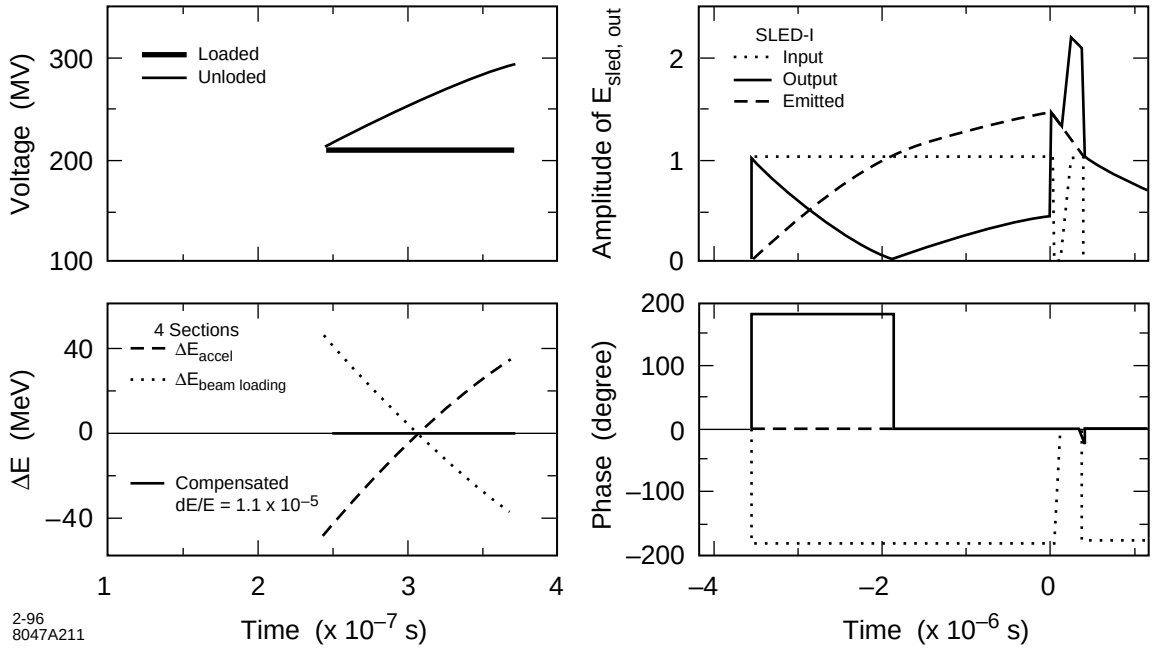

Figure 6-5. *Beam-loading compensation for a 2.2-A beam current in S-band linac by using amplitude modulation of the SLED-I wave form.*

band accelerator structure, the beam-loading voltage can be over 50% of the acceleration. The ΔF compensation is necessary for compensating such a high beam loading.

Since the linac is heavily loaded, short accelerator length is desirable, which can cut the power requirement for the klystrons as well as the cost of building the wrap-round solenoid. However, the length of the accelerator is limited by the maximum average gradient of the structure. Our criterion is that the average gradient in the L-band linac may not exceed 25 MV/m. In our design, we use two 5-m structures for acceleration and two 3-m structures for ΔF compensation. Two compensation sections operate at 1428 ± 1.428 MHz respectively to reduce the single-bunch effect. The filling time of the acceleration and compensation structures as simulated are 0.463 μs and 0.422 μs respectively. The compensation sections are required to have certain acceleration in order to reduce the gradient requirement for the acceleration sections. Each of the acceleration and compensation sections will be driven by two L75 klystrons and one SLED-I cavity. A schematic drawing of the e^+ capture linac is shown in Figure 6-6.

The acceleration klystrons will operate at 62.5-MW useful power while the compensation klystrons will operate at 47-MW useful power. This produces an average gradient for both the acceleration and compensation sections of about 25 MV/m, and a total energy gain of about 240 MeV. The center bunch runs 45° off-crest in the compensation sections, which provides a 53-MeV acceleration in each of the compensation sections. With the ΔF compensation, the beam-loading energy spread can be reduced to 0.82%, which is only a small fraction of energy spread in a single bunch. In Figure 6-12 are shown the energy spectrum of the beam-loading compensation and the SLED-I wave form for the capture linac.

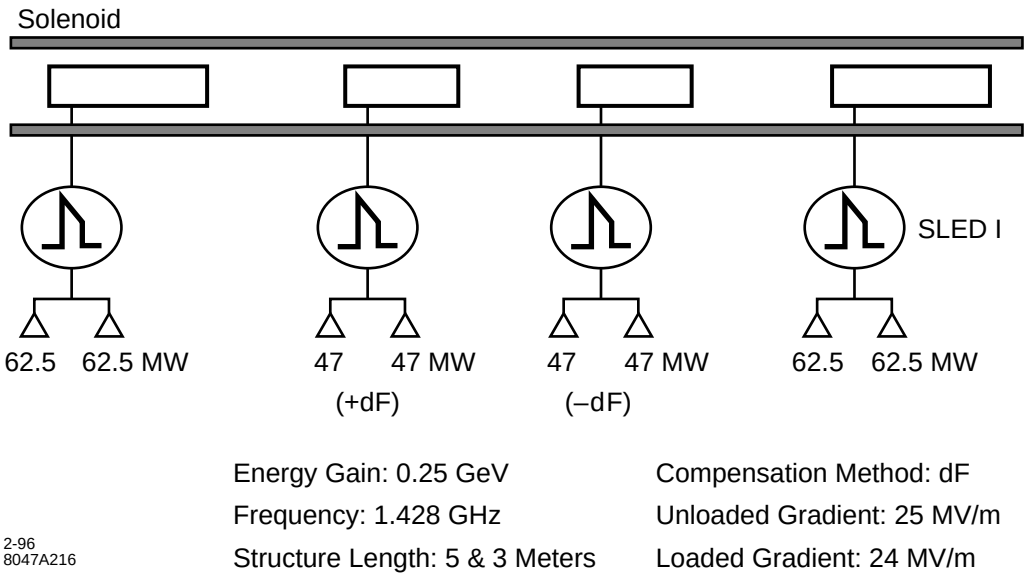

Figure 6-6. *The e^+ capture linac.*

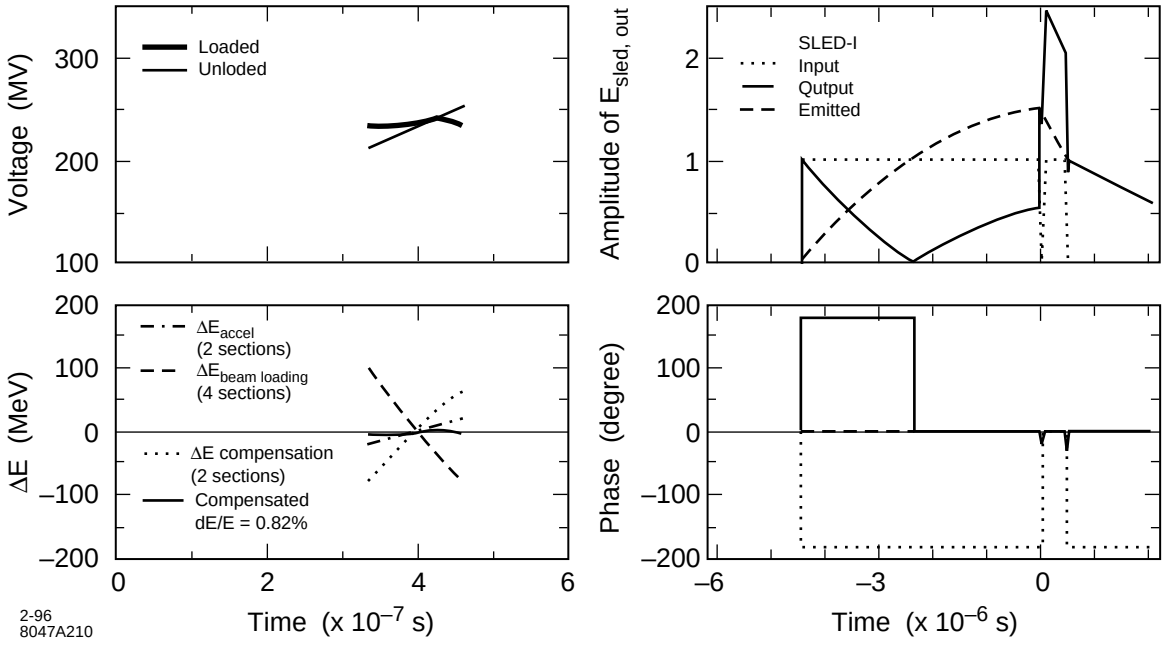

Figure 6-7. *Beam-loading compensation for the e^+ capture linac.*

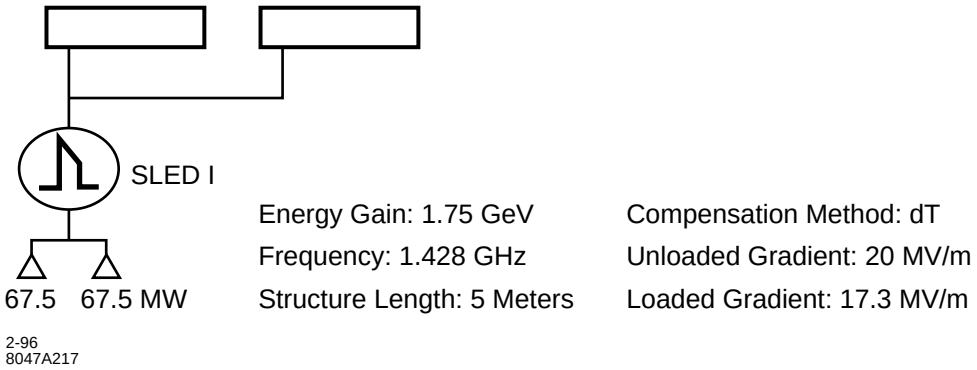

Figure 6-8. *An accelerator module for the e^+ booster linac.*

6.3.3 The e^+ Booster Linac

The e^+ booster linac accelerates the positron beam up to 2 GeV. The acceleration structure will be a detuned L-band structure ($F = 1.428$ GHz). The beam current in the linac is 2.75 A. The beam-loading compensation method is ΔT.

While the beam loading in the L-band structure is lower than in the S-band structure, beam-loading compensation still prefers a short filling time. The filling time of the L-band structure is chosen to be 0.675 μs. The beam loading is about 14% of the acceleration for a beam current of 2.75 A. Amplitude modulation of the SLED-I output is required to increase the derivative of the acceleration voltage. Two L75 klystrons will be used to drive one SLED-I cavity, which in turn drives two accelerator structures. An accelerator module is shown in Figure 6-8. The SLED-I wave form for the L-band accelerator is similar to Figure 6-5. The energy spread after beam-loading compensation is less than 5×10^{-5}. The loaded gradient of the structure is 17.3 MV/m.

6.3.4 L-band (e^-, e^+) Bunch Compressors

After the damping rings, the bunch length of the (e^+, e^-) beams is compressed. Two L-band linacs are used to produce the linear energy spread required for bunch length compression. The beam current is 1.6 A. The bunches run in phase quadrature with the rf crest phase. The compression voltage, which is the unloaded zero phase acceleration, is required to be 136 MeV and with less than 5% variation along the bunch train. The 5-m L-band detuned structures, same as the one used in the e^+ booster linac, will be used. Each compressor linac only needs two of such acceleration structures. Two L75 klystrons running at 35-MW useful power and one SLED-I cavity will be used to drive the whole L-band compressor linac. A schematic drawing is shown in Figure 6-9.

The beam-loading voltage is 90° off the rf voltage. Simple ΔT compensation method cannot be used for beam-loading compensation. A scheme that combines the ΔT method and phase modulation was studied, and shown to be effective for beam-loading compensation. The ΔT-amplitude modulation will be used for obtaining a uniform compression along the bunch train. A phase offset to the SLED-I output during the beam time is introduced to compensate the beam-loading voltage, which is 90° off-crest. The phase offset provides an in-phase (actually 180°-out-of-phase) component of rf voltage that cancels the beam-loading voltage.

Figure 6-10 shows the energy spectrum of the compressor linac and the SLED-I input and output wave forms. The amplitude and phase modulation of the SLED-I input can be obtained by properly phase-modulating the two klystrons.

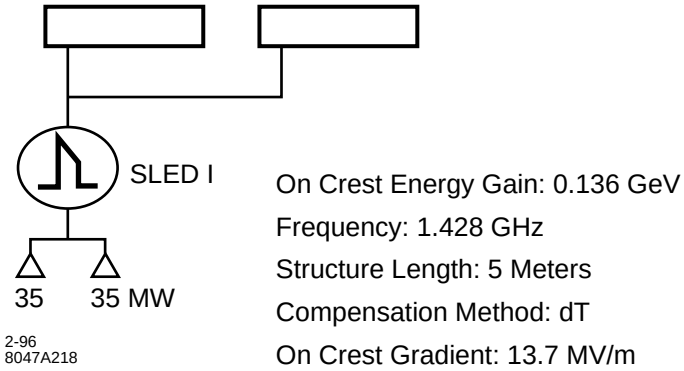

Figure 6-9. *An accelerator module for the L-band compressor linacs.*

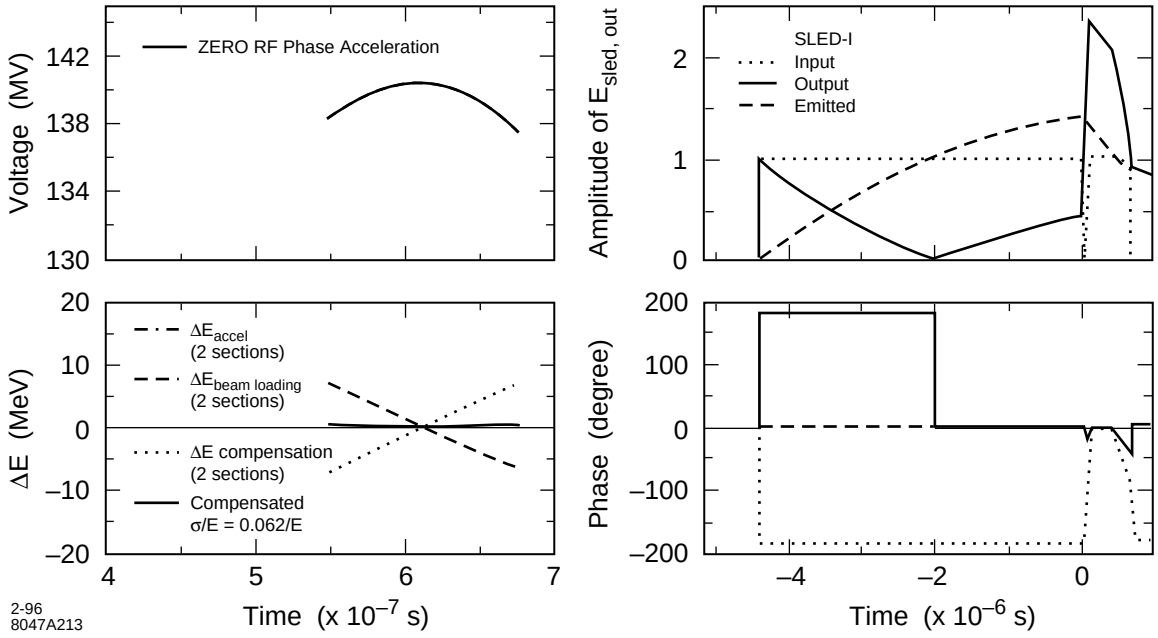

Figure 6-10. *Beam-loading compensation for the L-band compressor linacs.*

The amplitude modulation is obtained by modulating the phases of the two klystrons in opposite directions. Whereas, the phase offset is obtained by phase modulating the two klystrons in the same direction. The beam loading in these linacs can be reduced to $6\times10^{-2}/E_0$. The compression voltage deviates less than 3% along the bunch train.

6.3.5 S-band (e^-, e^+) Bunch Compressors

Before entering the main X-band linacs, the (e^+, e^-) beams are further compressed in bunch length in each of the respective accelerators. S-band linacs are used to produce the linear energy spread required for bunch length

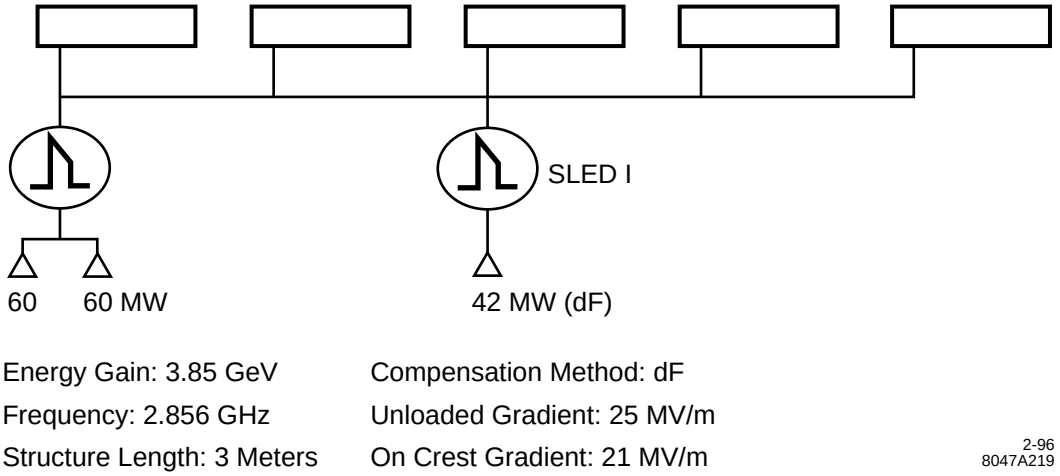

Figure 6-11. *An accelerator module for the S-band compressor linac. The four regular sections are used to generate a linear correlated energy spread within a bunch. One ΔF section is used to compensate the beam loading.*

compression. The beam current in these linacs is 1.5 A. The compression voltage, or the unloaded zero phase acceleration, is required to be 3850 MeV, and the deviation of the compression along the bunch train should be less than 5%. The beam loading in these linacs is relatively high. The ΔF sections will be used for beam-loading compensation, while the ΔT scheme will be used in the regular sections to obtain a uniform compression voltage. Both the ΔF and ΔT sections will be 3-m S-band DDS structures.

Two L65 klystrons and one SLED-I cavity will be used to drive four regular acceleration sections. Amplitude modulation of SLED-I output is needed to generate a uniform compression. The SLED-I wave form for the regular sections is shown in Figure 6-12. One L65 klystron and a SLED-I cavity will be used to drive one ΔF compensation section. The compensation klystron only needs to run at 42-MW useful power for an optimal beam-loading compensation. No amplitude modulation is needed for the compensation SLED-I. The ΔF sections operate alternatively at 2856 ± 1.1424 MHz through the linac to reduce the single bunch effect. A schematic drawing of an accelerator module as described above is shown in Figure 6-11.

In Figure 6-12 are shown the compression voltage and the beam-loading compensation results for an accelerator module. The optimal rf phase for the ΔF sections is 44° off-crest. At this rf phase, the ΔF sections also provide some acceleration that nearly cancels the deceleration (half the beam-loading voltage) due to the beam loading. With ΔF compensation, the beam-loading energy spread can be reduced to 0.62×10^{-3} at an energy of 10 GeV. The average gradient in the structure is about 22 MV/m.

An alternative ΔT compensation method, similar to the one used in the L-band compressors, was also investigated. It has been shown that the ΔT compensation can give better energy spectrum compared to the ΔF compensation. However, the ΔF method is more straightforward and operationally more convenient.

6.3.6 The (e^-, e^+) energy compressors

There are energy compressors associated with the electron and positron beams before they enter the damping rings. The compressor will be S-band for the electron beam and L-band for the positron beam. The compression voltage requirements for the S-band and L-band compressors are 42 MeV and 80 MeV respectively. The deviation of the

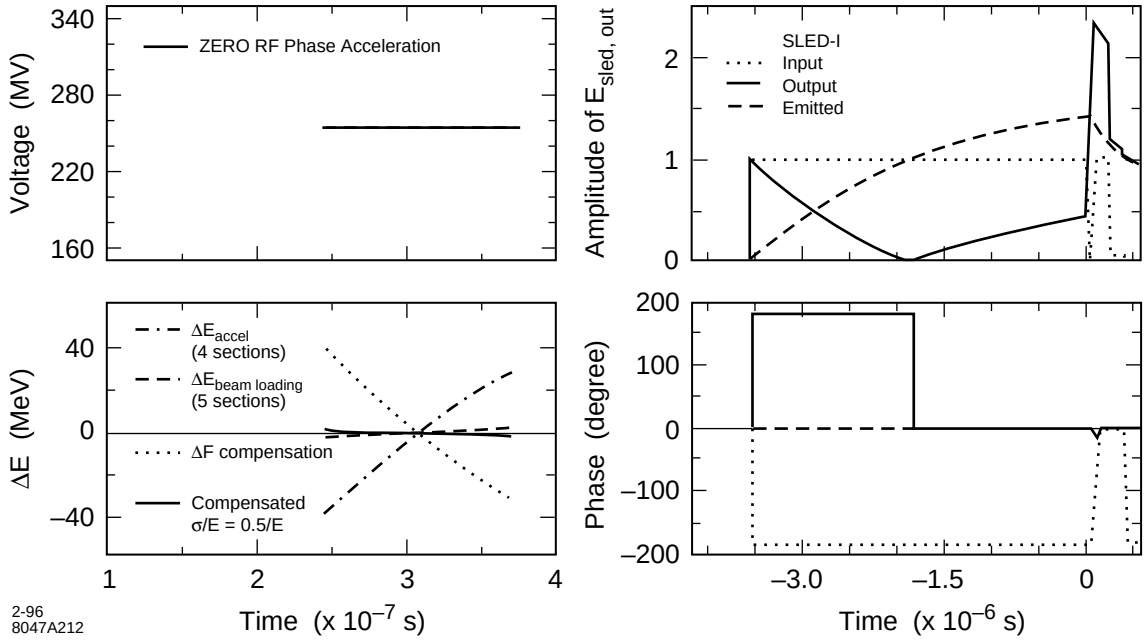

Figure 6-12. *Beam-loading compensation for the S-band compressor linacs.*

compression voltage along the bunch train is required to be less than 10%, and the compensated beam-loading energy spread less than 0.1% in full width. Both compressors will use ΔT and phase modulation method to obtain a uniform compression voltage and beam-loading compensation.

S-band e^- energy compressor. The beam current in the electron energy compressor is 2.2 A. A single 2.5-m S-band accelerator section is used to generate the energy correlation needed for energy compression. The filling time of the structure is 0.371 μs. The compressor will be driven by one unsledded S65 klystron, with a 130-ns rising time in amplitude. The maximum phase offset for beam-loading compensation is 60°. The resultant full energy spread along the bunch train is 0.73×10^{-3}, and the deviation of the compression voltage is less than 5%.

L-band e^+ energy compressor. The beam current in the positron energy compressor is 2.75 A. The compressor will be composed of one 4-m L-band accelerator section. The compressor will be driven by two L75 klystrons with SLED-I pulse compression. The filling time of the structure is 0.537 μs. The maximum phase offset for beam-loading compensation is 80°. With ΔT and phase modulation, the full energy spread can be reduced to less than 0.49×10^{-3} and the compression voltage is within 5% deviation.

6.3.7 Beam-loading Compensation in the Spare Modules

Each of the linacs discussed in this chapter is designed to have about 10% spare accelerating modules. The beam induces the same transient beam-loading voltage in these spare accelerator sections as in a powered section. In order to maintain localized compensation, we will drive one of the two klystrons which drives a module with a switched drive signal at $F_0 \pm \Delta F$. With appropriate choice of ΔF, 1.428 MHz for L-band and 1.1424 MHz for S-band, this drive frequency will produce enough voltage in the standard accelerating structures when powered by one klystron to compensate for the beam loading in the same structure. Since it is very unlikely that both klystrons in a module

	e^+ drive e^- booster	(e^-, e^+) prelinac	e^+ capture	e^+ booster	(e^-, e^+) L-band compressor		(e^-, e^+) S-band compressor	
					Bunch	Energy	Bunch	Energy
Frequency (GHz)	2.856	2.856	1.428	1.428	1.428	1.428	2.856	2.856
E Gain (GeV)	3-6, 2	8	0.250	1.75	0.136	0.080	3.85	0.042
Current (A)	2.2	1.5	14	2.75	1.6	2.75	1.5	2.2
$L_{\rm struct}$ (m)	3	3	5	5	5	4	3	2.5
T_f (μs)	0.371	0.371	0.464	0.675	0.675	0.537	0.371	0.371
N Struct/module	4	4	2	2	2	1	4	1
$P_{\rm klystron}$ (MW)	2×60/4	2×60/4	2×62.5/1	2×67.5/2	2×35/2	2×35/1	2×60/4	56[b]/1
Klystron Pulse (μs)	4	4	5	5	5	5	4	0.5
Average Gradient (MV/m)	17.3	21.2	24.2	17.3	13.7	20.0	21.1	16.8
(MV/module)	208	254	242	173	137	80.0	253	42
Compensation Method	ΔT	ΔT	$\Delta T/\Delta F$	ΔT	ΔT	ΔT	$\Delta T/\Delta F$	ΔT
$L_{\rm struct}$ (m)			3				3/3	
T_f (μs)			0.422				0.371	
N Struct/module			2				1	
$P_{\rm klystron}$ (MW)			2×47/1				42/1	
Klystron Pulse (μs)			5				4	
$\sigma/(\Delta E(\text{ MeV}))$	2.4×10^{-5}	1.1×10^{-5}	8×10^{-3}	5×10^{-5}	$\frac{0.062}{E_0}$	$\frac{0.49^a}{E_0}$	$\frac{6.2}{E_0}$	$\frac{0.73^a}{E_0}$

[a] Maximum energy spread.
[b] Not SLEDed.

Table 6-3. *A summary of low-frequency linac beam-loading compensation.*

will fail at the same time, this technique will usually maintain localized beam-loading compensation even with failed klystrons. Since ΔF is greater than the bandwidth of the SLED-I cavities, they will behave as if they are detuned.

6.3.8 Summary of the Beam-loading Compensation

A summary of the beam-loading compensation is shown in Table 6-3. In the compensation sections, the frequency offset ΔF is 1.428 MHz for the e^+ capture linac and is 1.1424 MHz for the S-band compressor linac. The notation, such as 2×60/4, in the klystron power specification means to use two klystrons running at 60-MW useful power to drive one SLED-I cavity, and the SLED-I cavity drives four accelerator sections.

Beam voltage	350 kV
Beam current	400 A
Rf pulsewidth @ rep rate	4 μs @ 180 Hz
Cathode loading	2:1 (8 A/cm2 max)
Cathode convergence	18:1 (3.525" dia.)
Rf output power	65 MW
Saturated gain	$\sim$55 dB
Efficiency	$\geq$40%
Operating frequency	2856 $\pm$1.4 MHz
3 dB Bandwidth	15 MHz
Solenoidal focusing field	1400 Gauss

Table 6-4. *Design parameters for a 65-MW S-band klystron*

Beam voltage	388 kV
Beam current	483 A
Rf Pulsewidth @ rep rate	5 to 6 μs @ 180 Hz
Cathode loading	2:1 (6 A/cm2 max)
Cathode convergence	11:1 (4" dia.)
Rf output power	75 MW
Saturated gain	$\sim$55 dB
Efficiency	$\geq$40%
Operating frequency	1428 $\pm$1.4 MHz
3 dB Bandwidth	8 MHz
Solenoidal focusing field	980 Gauss

Table 6-5. *Design parameters for a 75-MW L-band klystron.*

6.4 Klystrons

6.4.1 S-band S65 klystron

Klystrons operating at 2856 MHz with 65 MW of available rf output power will be required for the NLC. Such klystrons already exist at SLAC as the 5045 klystron tubes. The 5045 klystrons will need slight modifications to improve pulsewidth (from 3.5 μs to 4 μs) and average power handling capability. Table 6-4 summarizes the parameters for NLC S-band klystrons.

6.4.2 L-band L75 klystron

Klystrons operating at 1428 MHz with 75 MW of available rf output power will also be required for the NLC. Table 6-5 summarizes the parameters for NLC L-band klystrons. A conventional klystron as described above would be approximately 123-in long and weigh approximately 900 lb. Such a klystron can be built and operated using technology currently available and proven. Indeed, 150-MW klystrons operating at twice the frequency have already been built at SLAC. However, interesting designs for multiple-beam klystrons have been studied at SLAC which indicate a substantial reduction in beam voltage without sacrificing efficiency. For example, a 10-beam klystron operating at only 273 kV would have 114 A in each beam which leads to a theoretical efficiency of 64% (giving 200 MW).

6.5 Dipole Wakefields

The S-band accelerator sections will be detuned by about 6% in a Gaussian density distribution to diminish the effect of dipole wakefields. This will cause the structure to be what might inarticulately be called "over-constant-gradient", *i.e.*, the gradient rises from the input to the output. Damping will be desirable. A manifold damped structure similar to the X-band damped detuned structure is being studies and it appears to have dipole wakefields greatly reduced from the structure without damping. Figure 6-13 shows a MAFIA [Mafia Collab.] representation of 1/4 of a cell in the proposed three-m S-band structure. In order to enhance the damping, the S-band structure was modified from a simple scaling from the X-band design: a narrow (5-mm-wide) slot extends from each manifold into each disk, extending about half the distance from the manifold to the iris in the disk. This greatly enhances the coupling to the $TM11$-like mode which is predominant in the lowest dipole band for the parameters chosen for the S-band structure. The ringing time of microwave structure scales as $\lambda^{3/2}$, and consequently the natural scaling for accelerator structure length is $\lambda^{3/2}$. However, this scaling from the NLC X-band structure would give a cumbersome 14-m-long S-band accelerator section. Instead, a 3-m length has been chosen tentatively. With the filling time chosen for ΔT compensation, we get an average group velocity which is a factor of 2.2 smaller for the S-band structure. This change makes the lowest passband dipole predominantly $TM11$-like, even at the zero phase advance of the passband. Slots in the disks were added to improve the coupling. Narrow slots have negligible effect on the fundamental mode shunt impedance since they are parallel to the current for that mode.

A preliminary study indicates that just detuning will be adequate for the positron L-band linac because of the strong focusing produced by the many wrap-around quads and because of the very low dipole impedance of the large aperture L-band linac.

6.5.1 Detuned Structure

The most important wakefield in the S-band structure is the first passband dipole wakefields. One finds that by detuning the dipole frequency in a Gaussian density distribution, the wakefield can be dramatically suppressed. The NLC S-band structure will be detuned by about 6% in full width with a three-sigma cutoff. The detuning can be obtained by properly varying the iris aperture and the cell radius while keeping the fundamental frequency unchanged. Figure 6-14 shows a preliminary estimation of the dipole spectrum for the S-band structure. Each frequency shown in the spectrum corresponds to one cell in the structure.

The dipole wakefield estimated by using a equivalent circuit model [Thompson] for a S-band Gaussian detuned structure is shown in Figure 6-15. It is shown that the detuned structure can strongly suppress the wakefield. However,

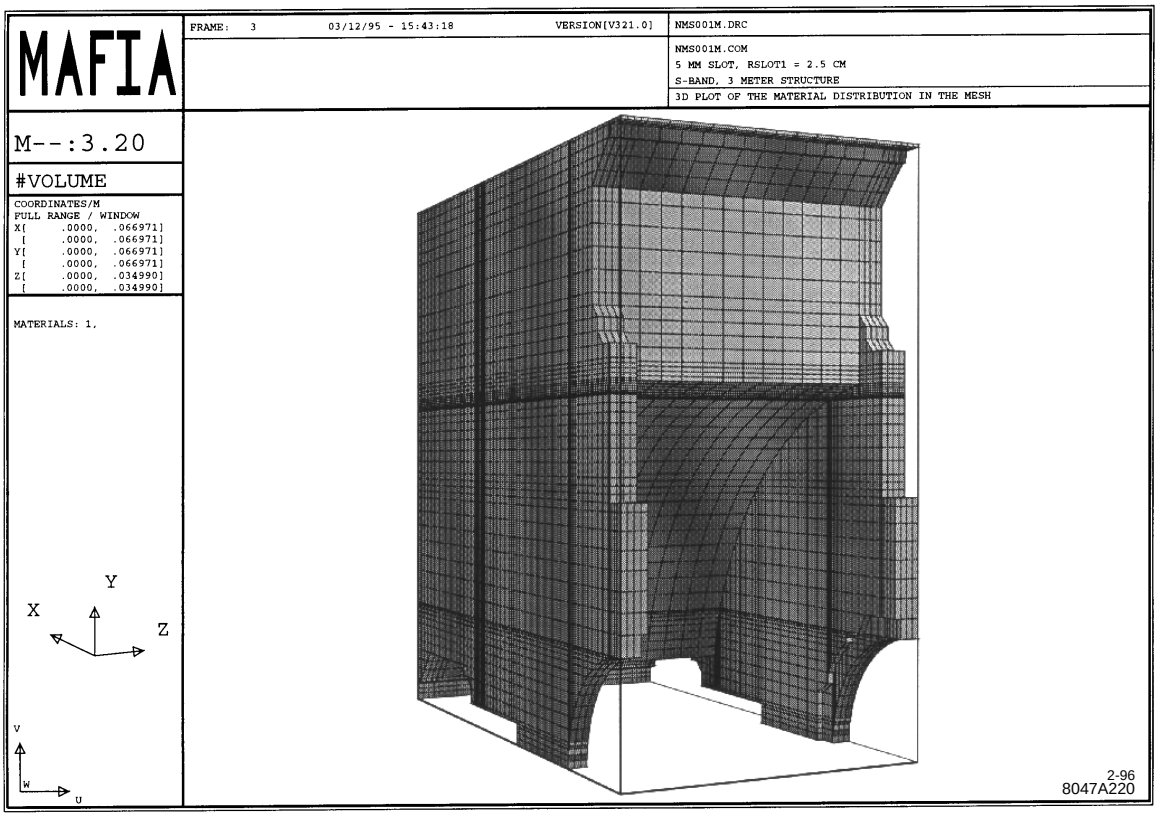

Figure 6-13. *The 1/4 cell of the S-band structure.*

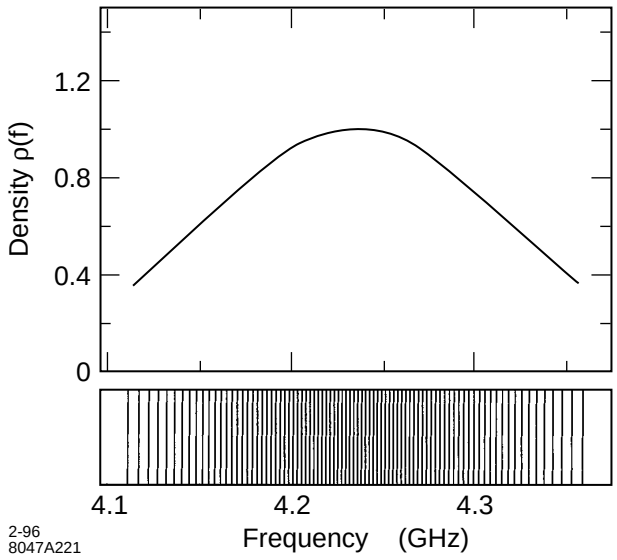

Figure 6-14. *Gaussian detuned dipole spectrum for the S-band structure.*

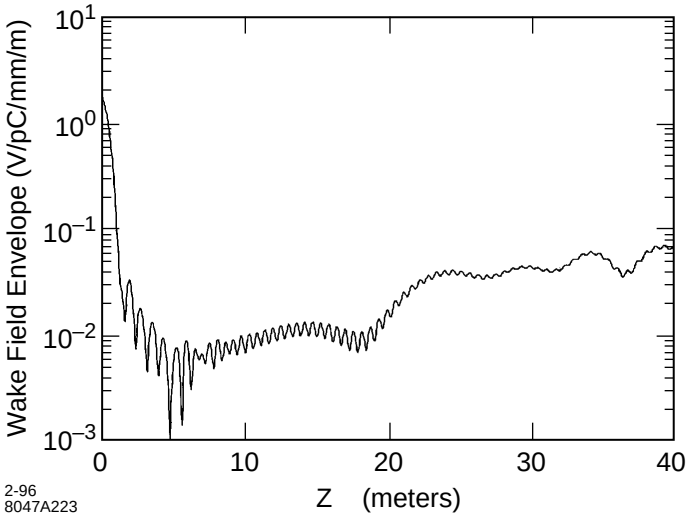

Figure 6-15. *Wakefields for a detuned S-band structure.*

since the dipole spectrum is a discrete and truncated Gaussian, the decoherence among the modes only helps to reduce the short-term wakefields. At a longer time scale, but shorter than the pulse length, the modes re-cohere, which results in strong long-term wakefields. Certain damping scheme is needed to minimize the long-term wakefields.

6.5.2 Damped Detuned Structure

A damping scheme similar to the X-band damping manifold will be used to damp the long-term dipole wakefield. In addition to the damping manifold, a narrow slot extends from each manifold into each disk is added to enhance the coupling, see Figure 6-16. The manifold runs parallel to the structure, and is 1.39-cm wide and 2.12-cm high. The wall between the cell and the manifold is cut open with the full manifold width. The narrow slot, 0.5 cm in full width, cuts about halfway into the disk. The full height of the slot-manifold is about 3.834 cm.

The coupling between the slot-manifold and the cell is estimated by use of the 3-D MAFIA and code MDAMP [Kroll 1994] derived from the equivalent circuit model. For a Gaussian detuned structure, the iris radii a and the cell radii b are tapered. With the additional slot-manifold, the structure is three-dimensional. It is not practical to model the whole structure by use of the 3-D MAFIA. However, since the tapering is gradual and smooth, we can use a cell-to-cell approach, *i.e.,* to model the structure cell by cell. For each cell, the two irises at the two ends of the cell are assumed to have the same radius, which takes the average of the two actual radii of the irises. Periodic boundary conditions are applied to the two ends, which is equivalent to model an infinitely long constant impedance structure. The 3D MAFIA is used to model a number of selected cells along the structure. Interpolation method is used to obtain the parameters for the rest of the cells.

In Figure 6-17 is shown a MAFIA result of the dispersion relation for a cell with $a = 1.150$ cm and $b = 4.071$ cm. At zero phase advance, the lower frequency mode is the manifold mode and the upper mode is the dipole mode of the cell. As the phase advance increases, the two modes come closer to each other. The modes, however, do not cross. At a particular phase advance, 120° for this case, the field patterns of these modes switch and the dispersion curves start to separate further apart. The frequency separation of the modes at the avoided crossing point indicates the coupling

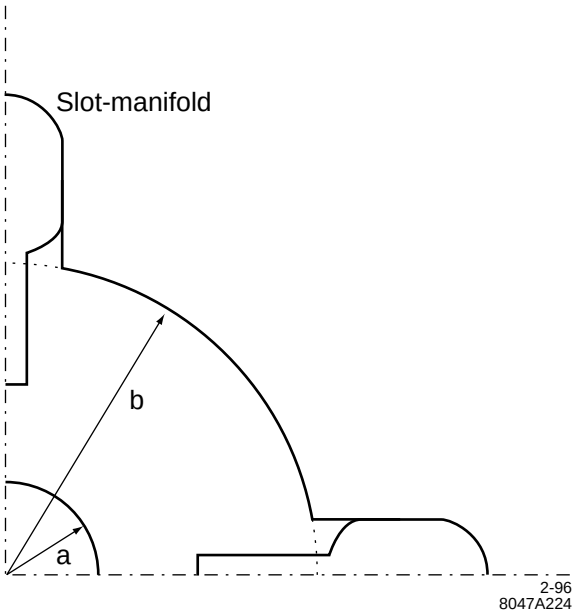

Figure 6-16. *Slot-manifold damping structure for the S-band accelerator.*

strength, with large separation corresponding to large coupling. The simulation shown in Figure 6-17 has about 6% of coupling.

The coupling is insensitive to the width of the slot. In Figure 6-18 are shown the couplings for different slot widths. As one can see that the coupling only increases by 0.5%, from 5% to 5.5%, as the slot width increases from 3 mm to 5 mm. On the other hand, the coupling is sensitive to the depth of the slot. We calculated the couplings for different slot positions while keeping the whole slot-manifold geometry unchanged. Figure 6-19 shows the coupling as a function of the nearest distance of the slot to the axis. The coupling varies almost linearly to the distance and the slope is about 1% per millimeter.

The coupling not only depends on the depth of the slot, but also depends on the iris opening. The iris opening is tapered in the detuned S-band structure, with large opening in the front and smaller opening toward the end. The radial position of the slot will also be tapered to get similar coupling for all cells.

The slot-manifold also preserves the Q_0 and the shunt impedance (r) of the structure, as shown in Figure 6-18. The reason underlying this is the small wall loss of the fundamental mode induced by the slot. Even though the slot-manifold couples strongly to the $TM11$ dipole field, it has very weak coupling to the fundamental mode which is a $TM01$ mode. For the $TM01$ mode, the current in the disk is in the radial direction. The narrow radial slot in the disk has small perturbation to this current. The E and B fields of the fundamental mode are weak in the slot, which results in small wall loss and associated Q_0 and r loss.

The dipole wakefield, estimated by using equivalent circuit model, for a damped-detuned structure with 6% cell-manifold coupling is shown in Figure 6-20. The long-term wakefield is strongly minimized by the damping structure. This indicates that the slot-manifold can provide the coupling needed for damping the wakefields.

It is worthwhile to mention that the equivalent circuit model used so far is the single-band model. Recently, a multi-band equivalent circuit model has been developed, which promises to give better accuracy for wakefield estimation.

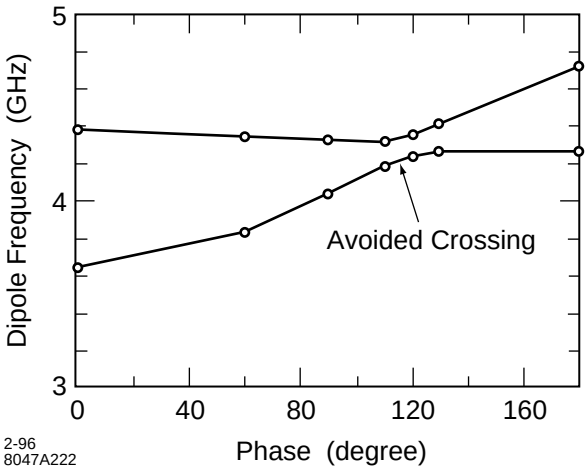

Figure 6-17. *MAFIA simulation of the dispersion curve of a slot-manifold coupled S-band accelerator cell. The avoided crossing indicates the strength of the coupling.*

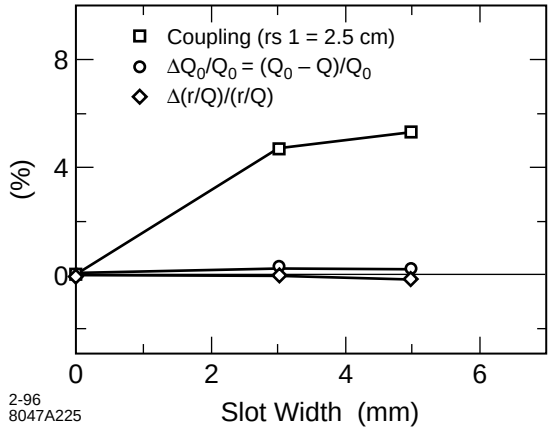

Figure 6-18. *Cell-slot-manifold coupling, $\Delta Q_0/Q_0$ and $\Delta(r/Q_0)/(r/Q_0)$ for different slot width.*

Nevertheless, the single-band model has been proven experimentally in the X-band damped-detuned structure measurements to give reasonably good results.

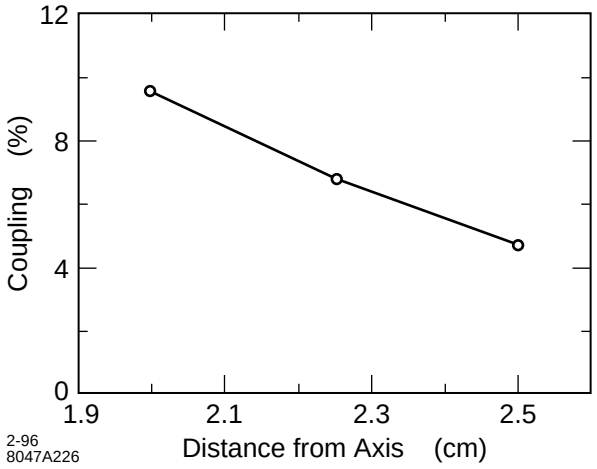

Figure 6-19. *Cell-slot-manifold coupling as a function of the distance of the slot from the axis.*

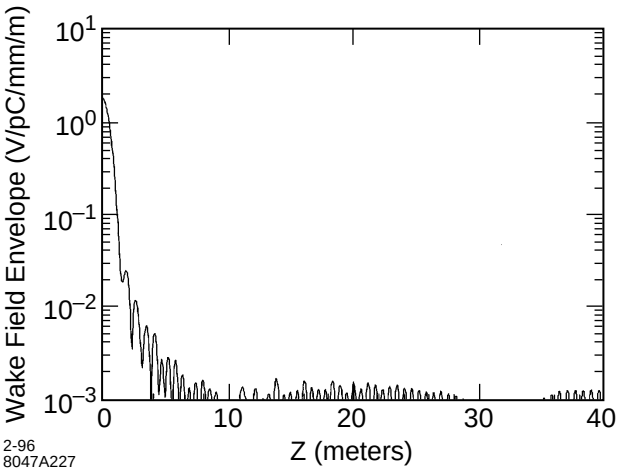

Figure 6-20. *Wakefields for a damped-detuned S-band structure.*

References

[Mafia Collab.] The Mafia Collaboration, MAFIA—The ECAD System.

[Thompson] K. Thompson, private communications.

[Kroll 1994] N. Kroll *et al.*, "Manifold Damping of the NLC Detuned Accelerating Structure", SLAC–PUB–6660 (1994), in Proc. of the Sixth Workshop on Advanced Accelerator Concepts, Lake Geneva, WI, June 12-18, 1994.

Contributors

- David Farkas
- Kwok Ko
- Zenghai Li
- Roger Miller
- Tor Raubenheimer
- Daryl Sprehn
- Huan Tang
- Kathy Thompson
- Dian Yeremian